Grain size effect on deformation mechanisms in Mg-3Gd

Luo, X.; Luo, J. Q.; Feng, Z. Q.; Hu, F. P.; Yu, T.; Berggreen, C.; Wu, G. L.; Hansen, N.; Huang, X.

Published in:
I O P Conference Series: Materials Science and Engineering

Link to article, DOI:
10.1088/1757-899x/580/1/012040

Publication date:
2019

Document Version
Publisher's PDF, also known as Version of record

Grain size effect on deformation mechanisms in Mg-3Gd

IOP Conf. Series: Materials Science and Engineering **580** (2019) 012040 doi:10.1088/1757-899X/580/1/012040

Grain size effect on deformation mechanisms in Mg-3Gd

X Luo [1], J Q Luo [1], Z Q Feng [1], F P Hu [1], T Yu [2], C Berggreen [2], G L Wu [1], N Hansen [1,3] and X Huang [1,2]

[1] Joint International Laboratory for Light Alloys (MOE), College of Materials Science and Engineering, Chongqing University, Chongqing 400044, China
[2] Department of Mechanical Engineering, Technical University of Denmark, DK-2800, Kgs, Lyngby, Denmark
[3] Technical University of Denmark, Risø Campus, DK-4000 Roskilde, Denmark

Email: wugl@cqu.edu.cn

Abstract. Mg-3Gd (wt. %) samples were prepared by accumulative roll-bonding (ARB) and subsequent annealing to produce samples with average grain sizes in a wide range from 3.3 μm to 45.1 μm. These samples were tensile tested at room temperature. Dislocation structures and deformation twins in the tested tensile samples were characterized by transmission electron microscopy. Dislocations with different types of Burgers vector were identified based on two-beam diffraction contrast experiments. The results revealed that deformation twins and <a> dislocations are dominant in coarse-grained samples while <c+a> and <a> dislocations characterize the fine grain deformation structure. The transition of deformation mechanisms and its implications for microstructural design and property optimization are discussed.

1. Introduction

Compared to cubic metals, the lower crystallographic symmetry of hexagonal close-packed (HCP) magnesium with c/a ratio of 1.624 results in high plastic anisotropy and unique mechanical characteristics [1, 2]. The high anisotropy in magnesium alloys usually results in a high critical resolved shear stress (CRSS) ratio between non-basal and basal slip, and basal slip and twinning act as dominant deformation modes [1-4]. However, some non-basal slip is expected, as it is necessary to accommodate the strain along c-axis in order to achieve the five independent deformation systems required for an arbitrary deformation [5, 6]. Therefore, the activation of non-basal slip systems is extremely important for highly ductile magnesium alloys.

The addition of rare earth elements, such as Gd and Y, into magnesium can change the CRSS and the core structure for <c+a> dislocations [7], thereby improving the ability to activate <c+a> slip [8]. In contrast to the effect of rare earth elements in magnesium alloys [9], current experimental and simulated results for fine-grained magnesium alloys with high ductility suggest that more controversy lies in understanding the grain size effect [10]. The deformation mechanisms in coarse-grained magnesium alloys at room temperature are dominated by basal <a> slip and twinning [1, 2]. However, due to the restraint of deformation twinning in fine-grained magnesium alloys, it is considered more slip systems are likely to be activated [11, 12]. Therefore, our hypothesis is that the control of grain size provides the opportunity to activate multiple slip systems. In this work, we prepared coarse-grained and fine-grained Mg-3Gd samples by accumulative roll-bonding (ARB) and subsequent annealing, and carried out

detailed electron microscopy observations to identify the grain size effect on the activation of <a> slip, <c+a> slip and twinning.

2. Experimental

An Mg-3%Gd ingot with a diameter of 100 mm was prepared by semi-continuous casting, followed by homogenization treatment at 450 °C for 24 h. The homogenized ingot was then subjected to hot extrusion to a 3 mm thick plate, hot rolling to 1 mm sheet in thickness at 450 °C, and finally annealing at 500 °C for 3 h. After annealing the initial sheet samples show a coarse grain structure and a weak basal texture. The annealed sheet was sparking-machined into specimens with a length of 70 mm and a width of 25 mm, which were then processed by the ARB technique [13] for two cycles. The ARB samples were finally annealed between 310 °C and 500 °C for 1 h to prepare samples with average grain sizes ranging from 3.3 μm to 45.1 μm.

Dog-boned tensile specimens with a gauge length of 13 mm and cross section of 5×1 mm^2 were cut from the annealed samples. Uniaxial tensile tests were performed in a Shimadzu AGX-50 testing frame at a strain rate of 8.3×10^{-4} s^{-1} at room temperature. The tensile direction was parallel to the rolling direction (RD) of the ARB-processed sheets.

The microstructures of the annealed samples were characterized by electron backscatter diffraction (EBSD) in a Zeiss Auriga scanning electron microscope equipped with an Oxford Aztec EBSD detector. The samples for EBSD analyses were first mechanically polished and then electrochemically polished in the Struers AC2 solution. Tensile tested samples were also characterized in a JEM-2100 transmission electron microscope (TEM). TEM foil samples were cut in longitudinal section (RD-ND section; ND being the normal direction) from the uniformly elongated area of each tested tensile samples. The foils were prepared by ion milling after mechanical grinding to 100 μm thickness. Dislocation contents of individual grains were analyzed in the TEM under two-beam diffraction conditions using different diffraction vectors ***g***.

3. Results and discussion

Figure 1 shows EBSD boundary maps of the annealed and initial samples. After annealing for 1 h at 310 °C and 360 °C, the material is fully recrystallized samples with average grain sizes of 3.3 μm and 6.3 μm, as shown in figures 1a and b. Figure 1c shows the microstructure of the initial sample with an average grain size of 45.1 μm. Note that low concentration of low-angle boundaries (marked by green lines) are observed within recrystallized grains.

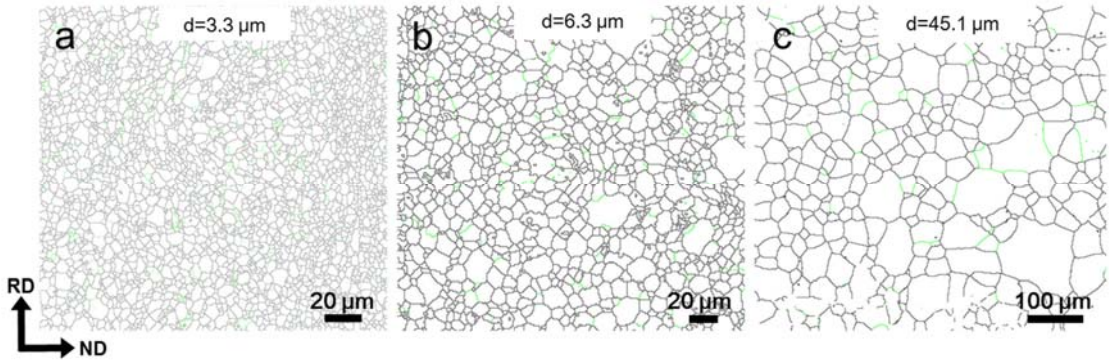

Figure 1. EBSD boundary maps showing the grain structures of (a, b) two fine-grained samples produced by ARB processing followed by annealing for 1 h at (a) 310 °C and (b) 360 °C, and (c) the initial sheet sample, where high-angle boundaries above 15° are drawn in black, and low-angle boundaries between 2° and 15° are drawn in green.

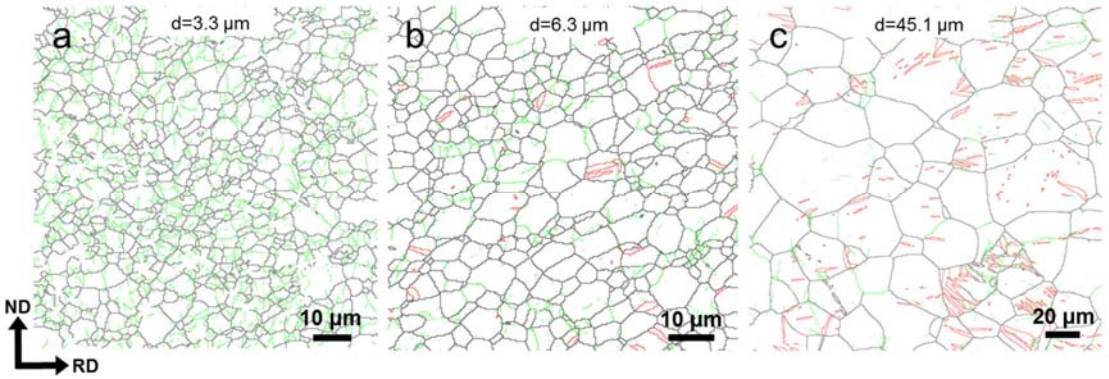

Figure 2. EBSD boundary maps showing microstructures of 5% tensile deformed samples (a) 310 °C 1h, (b) 360 °C 1h and (c) initial sample, where high-angle grain boundaries above 15° are drawn in black, low-angle boundaries between 2° and 15° are drawn in green, and twin boundaries are drawn in red.

EBSD results of fine-grained and coarse-grained samples after deformation to a tensile strain of 5% are shown in figure 2, where the boundaries with misorientation angles above 15° (high angle boundaries; HABs), between 2° to 15° (low angle boundaries; LABs) and twin boundaries 86° (TBs) are indicated by black, green and red lines, respectively. As shown in figures 2a and b, a high concentration of LABs (marked by green lines) is found in fine grains. In contrast within coarse grains in figure 2c, many twins (marked by red lines) are formed, with only a low concentration of LABs.

Figure 3 illustrates TEM images of a fine-grained sample tensile-deformed to failure. Many dislocations were activated during tensile deformation. In figure 3a, the two-beam dark field (TBDF) TEM image with g=[0002] near the $[01\bar{1}0]$ zone axis shows a mass of visible dislocations inside the grain, and all these dislocations show a c-component Burgers vector, e.g. <c+a> and <c>. The TBDF TEM image using g=$[2\bar{1}\bar{1}0]$ near the $[01\bar{1}0]$ zone axis also shows lots of dislocations (see figure 3b), and these dislocations are identified as <c+a> (marked by red dashed arrows) and <a> type (marked by white dashed arrows). Moreover, all dislocations are visible in figure 3c. Note the basal plane is indicated by white solid line in figure 3c. In order to distinguish different dislocation types clearly, a sketch stored all dislocations remained in this deformed grain is given in figure 3d. Red and white lines in figure 3d represent the <c+a> and <a> dislocations respectively. After careful observation, it is revealed that dislocation-based deformation mechanisms including <c+a> and <a> slip dominate in fine-grained samples during tensile deformation.

Figure 4 illustrates TEM images of coarse-grained sample tensile deformed to failure showing typical twin and dislocation structures. Based on selected area electron diffraction (SAED) analysis (see inset in figure 4a), it was found that deformation twinning and parallel stacking faults (SFs marked by red solid arrows) were activated. Note the basal plane is indicated by white solid line. Parallel <a> dislocations are also found and are indicated by white dashed arrows in figure 4a. A sketch showing dislocations and SFs corresponding to the rectangular region in figure 4a is given in figure 4b. White and red solid lines in figure 4b represent <a> dislocations and SFs respectively. From the TEM observations described above, it is seen that deformation mechanisms including deformation twinning and <a> slip dominate in coarse-grained samples during tensile deformation.

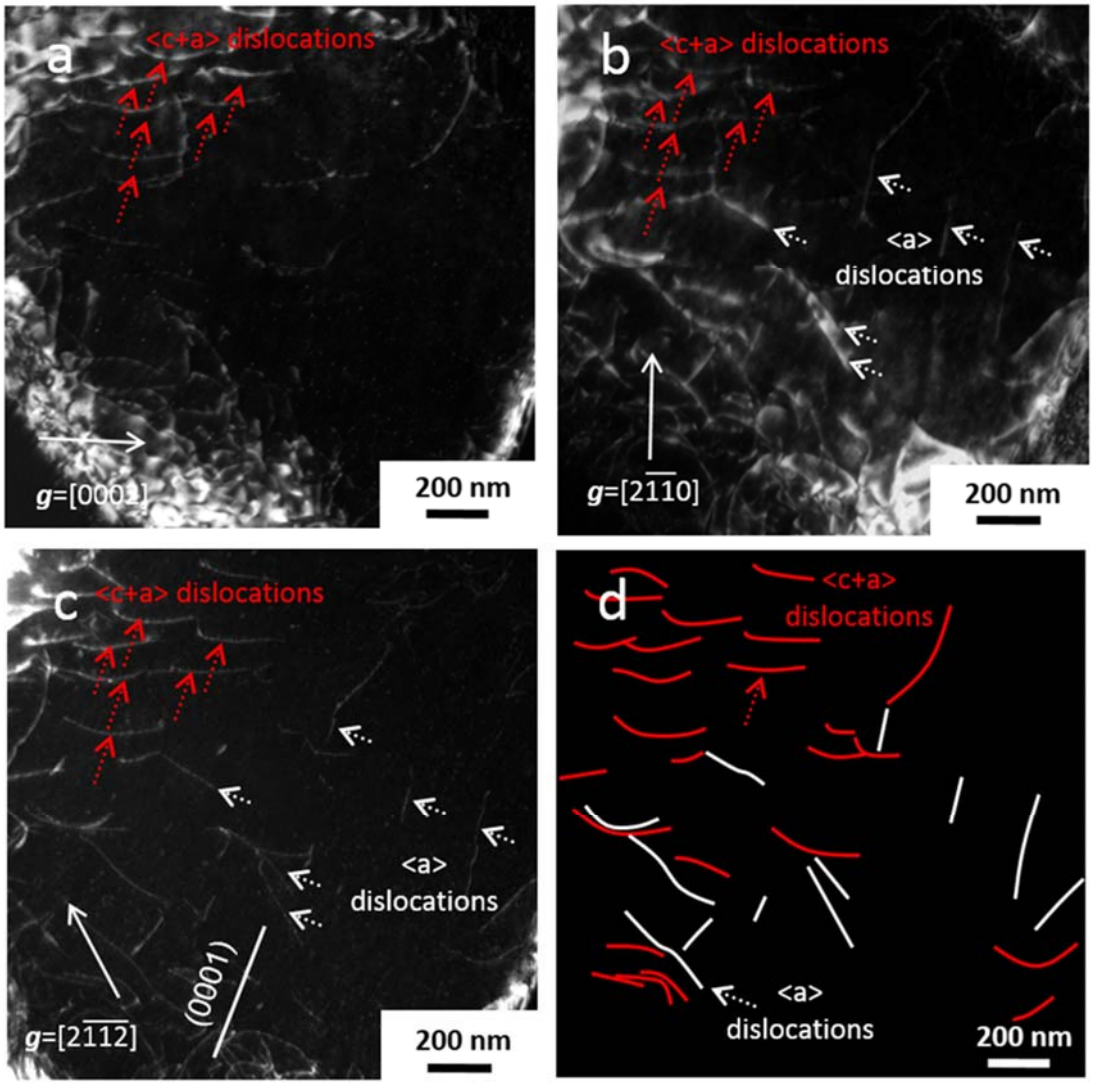

Figure 3. TEM images of fine-grained sample tensile deformed to failure; (a, b, and c) are TBDF images with g=[0002], g=[2$\bar{1}$10] and g=[2$\bar{1}\bar{1}$2]], respectively, near the [01$\bar{1}$0] zone axis; (d) a sketch showing all dislocations identified in this grain.

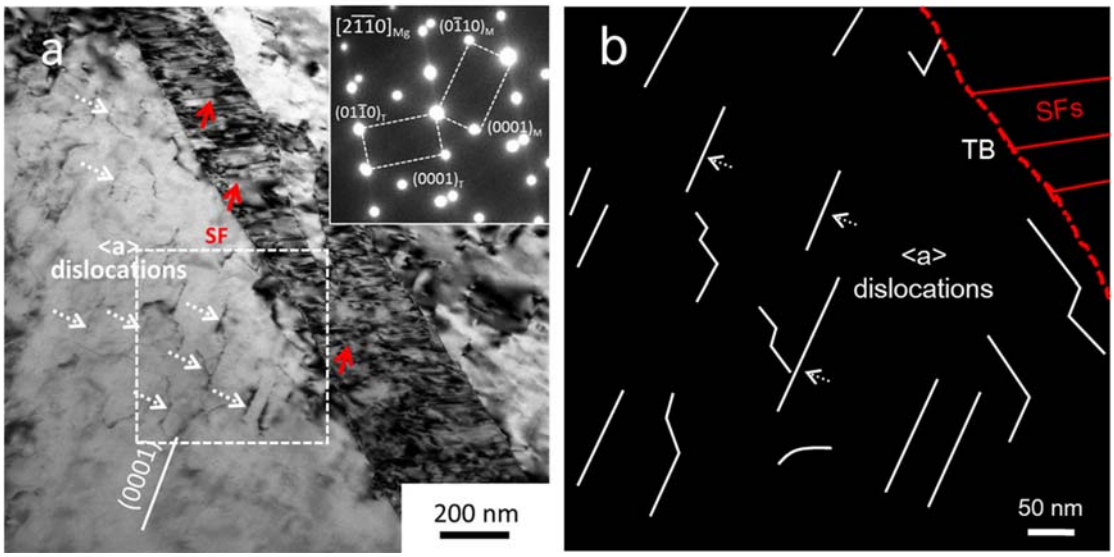

Figure 4. TEM image of coarse-grained sample tensile deformed to failure showing the activation of deformation twinning and <a> dislocations.

In summary, a transition in deformation mechanisms from deformation twinning and <a> slip in coarse grain structures to <a> and <c+a> slip in fine grain structure was confirmed by both EBSD and TEM observations. In contrast with normal <a> slip in conventional coarse-grained magnesium alloys, <c+a> slip shows stronger multiplication, interaction and cross-slip ability, which not only lead to a high work hardening rate but also improve slip distance and dislocation density. Furthermore, the activation of multiple slip systems in fine-grained samples may transform the typically highly anisotropic deformation of magnesium alloys to a more homogeneous deformation mode, similar to fcc and bcc metals, such as Al and IF steel [14, 15]. The abnormally active <c+a> slip in fine grains help, therefore, to ensure homogeneous deformation and satisfy the von-Mises condition during plastic forming of magnesium alloys.

4. Conclusions

The grain size dependence of the transition in deformation mechanisms, from twinning and <a> slip to <c+a> and <a> slip based plasticity, has been investigated by tensile deformation of Mg-3Gd with a grain size in the range 3.3 to 45.1 um. A transition marking change of dislocation types from <a> in a twinned structure at large grain size, to <a> and <c+a> in small grains was confirmed. The transition of deformation mechanisms and its implications for microstructural and property optimization highlight the scope for advanced design of magnesium alloys through structural refinement to a fine grain size.

Acknowledgements

This work was sponsored by the State Key Research and Development Program of Ministry of Science and Technology (MOST) of China (2016YFB0700401, 2016YFB0700403) and National Natural Science Foundation of China (No. 51471039, 51501022, 51327805). Part of this research was conducted using mechanical testing equipment from DTU Center for Advanced Structural and Material Testing (CASMAT), Grant No. VKR023193 from Villum Fonden. TY thanks the European Research Council (ERC) under the European Union's Horizon 2020 research and innovation programme (grant agreement No 788567). NH thanks the support of the "111" Project (B16007) by the Ministry of Education and the State Administration of Foreign Experts Affairs of China.

References

[1] Christian J W and Mahajan S 1995 *Prog. Mater. Sci.* **39** 1-157
[2] Agnew S R and Duygulu Ö 2005 *Int. J. Plasticity* **21** 1161-93
[3] Chapuis A and Driver J H 2011 *Acta Mater.* **59** 1986-94
[4] Staroselsky A and Anand L 2003 *Int. J. Plasticity* **19** 1843-64
[5] Koike J, Kobayashi T, Mukai T, Watanabe H, Suzuki M, Maruyama K and Higashi K 2003 *Acta Mater.* **51** 2055-65
[6] Zhang D, Jiang L, Schoenung J M, Mahajan S and Lavernia E J 2015 *Philos. Mag.* **95** 3823-44
[7] Ding Z, Liu W, Sun H, Li S, Zhang D and Zhu Y 2018 *Acta Mater.* **146** 265-72
[8] Sandlobes S, Zaefferer S, Schestakow I, Yi S and Gonzalez-Martinez R 2011 *Acta Mater.* **59** 429-39
[9] Basu I, Pradeep K G, Mießen C, Barrales-Mora L A and Al-Samman T 2016 *Acta Mater.* **116** 77-94
[10] Wu Z, Ahmad R, Yin B, Sandlöbes S and Curtin W A 2018 *Science* **359** 447-52
[11] Meyers M A, Vöhringer O and Lubarda V A 2001 *Acta mater.* **49** 4025-39
[12] Fan H, Aubry S, Arsenlis A and El-Awady J A 2016 *Scripta Mater.* **112** 50-53
[13] Saito Y, Utsunomiya H and Tsuji N 1999 *Acta Mater.* **47** 579-83
[14] Kamikawa N, Huang X, Tsuji N and Hansen N 2009 *Acta Mater.* **57** 4198-208
[15] Huang X, Kamikawa N and Hansen N 2010 *J. Mater. Sci.* **45** 4761-69